Heliyon 9 (2023) e13805

Contents lists available at ScienceDirect

Heliyon

journal homepage: www.cell.com/heliyon

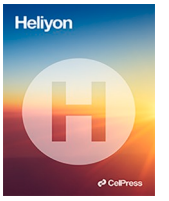

Research article

Research on high efficiency and high dynamic optimal matching of the electro-hydraulic servo pump control system based on NSGA-II

Mingkun Yang [b], Guishan Yan [a,*], Yuhang Zhang [b], Tiangui Zhang [b], Chao Ai [b]

[a] School of Intelligent Systems Engineering, Sun Yat-Sen University, Guangzhou, 510275, China
[b] School of Mechanical Engineering, Yanshan University, Qinhuangdao, 066004, China

ARTICLE INFO

Keywords:
Electro-hydraulic servo pump control system
High dynamic
Efficient energy-saving
Multi-objective optimization
NSGA-II

ABSTRACT

An electro-hydraulic servo pump control system (hereinafter referred to as EHSPCS) is a volume servo control unit that is highly integrated with servo motors, fixed-displacement pumps, hydraulic cylinders and functional valve groups. Because of its unique volume direct-drive control mode, the dynamic performance of the system is limited, and the thermal power loss is large, which seriously restricts the improvement of the working quality of the system. To improve the dynamic performance of the system and reduce the thermal power loss to the maximum extent, a multi-objective optimization design method for the EHSPCS is proposed by comprehensively considering the dynamic and efficient energy-saving characteristics of the system. The evaluation model of the dynamic period of the hydraulic cylinder and the thermal power loss of the servo motor are given. Parameters such as the electromagnetic torque of the servo motor, displacement of the hydraulic pump, and working area of the hydraulic cylinder are intelligently optimized by a non-dominated sorting genetic algorithm with elite strategy (NSGA-II). The Pareto front of multi-objective optimization and the corresponding Pareto solution set are obtained; thus, the optimal matching of the system characteristics is realized. Finally, the relevant theory of the multi-objective optimization algorithm is applied to optimize the performance parameters of the hydraulic servo motor, and the prototype is tested in engineering. The experimental results show that the dynamic period of the hydraulic servo motor is accelerated after optimization, and the thermal power loss is significantly reduced. The dynamic and efficient energy-saving characteristics of the system are improved, which further verifies the feasibility of the proposed theory.

1. Introduction

An EHSPCS has the advantages of efficient energy-saving and high power-weight ratio [1,2]. It is widely used in high-precision control fields, such as aircraft rudder control [3], hydraulic excavator arm drive systems [4], and wind variable propeller control [5]. However, owing to the large inertia of the servo motor and fixed-displacement pump, and the time delay of the volume servo speed regulation response, the static accuracy of the system is not high and the dynamic performance is limited. Simultaneously, owing to the high integration of the EHSPCS, the heat dissipation capacity of the system is weak, and the thermal power loss is serious. Therefore efficient energy-saving and dynamic characteristics are key indicators for measuring the performance of the EHSPCS. However, these

* Corresponding author.
E-mail address: yangsh235@mail.sysu.edu.cn (G. Yan).

https://doi.org/10.1016/j.heliyon.2023.e13805
Received 21 December 2022; Received in revised form 9 February 2023; Accepted 13 February 2023
Available online 18 February 2023

two indicators often contradict each other and have a complex nonlinear relationship with the design parameters, which is a multi-objective optimization problem. It is necessary to consider how to calculate it eclectically to optimize the comprehensive performance of the system. So it is of great significance to study the optimal matching of the EHSPCS performance indicators.

An EHSPCS is a complex system with multiple variables, strong coupling, and nonlinearity. Aiming at the research on the dynamic characteristics of the system, Li [6] studied and analyzed the influence of motor output torque and other factors on the dynamic characteristics of the system, and adopted relevant control strategies to improve the dynamic characteristics of the EHSPCS. Lee [7,8] proposed a new type of EHSPCS that solved the problem of flow asymmetry through redundant actuators and then improved the dynamic characteristics of the system. Based on the internal control mechanism of the EHSPCS, Jiang [9] analyzed the dynamic response characteristics of the current loop, velocity loop, position loop and pressure loop of the system, the research results showed that the position/force control of the system can obtain good dynamic response and steady-state accuracy after the parameters are determined on the basis of the dynamic analysis of the control loop. In order to solve the motor heating problem of EHSPCS electric power steering system and the contradiction between high dynamics and high efficiency, Huang [10] proposed a new active load sensing principle and structure of electric power steering system based on the principle of load sensing. While effectively reducing the heating of the motor, it ensures the dynamic performance of the system. Aiming at the research on the efficient energy-saving characteristics of the thermal power loss of the system, the relevant scholars [11–13] analyzed the heat transfer and heat dissipation mechanism of the EHSPCS, established the corresponding thermodynamic model, and studied the thermal power loss law of the components; Qu [14] proposed an efficient solution of a linear drive EHSPCS, which can improve the energy-saving performance of the system by energy regeneration and recovery beyond the load. McCullough [15] analyzed the temperature rise caused by energy loss and summarized the influence of oil temperature on the leakage coefficient, damping coefficient, and other important parameters of the system.

With regard to multi-objective optimization, researchers have used artificial neural networks [16] and Kriging approximate model technology [17] and so on to construct approximate models. The particle swarm optimization algorithm (PSO) [18], butterfly algorithm [19], simulated annealing algorithm (SA) [20], and non-dominant sorting genetic algorithm with elite strategy (NSGA-II) [21,22] were used to optimize the parameters of related systems. Subsequently, the analytic hierarchy process (AHP) [23], TOPSIS entropy weight [24], and other comprehensive decision-making methods were applied to set the weight between multiple objectives and select the optimal design scheme. Finally, experiments and simulation platforms were built to verify the multi-objective optimization results.

The above research has carried out relevant survey and analysis on the dynamic characteristics, thermal power characteristics and other inherent characteristics of the EHSPCS and the multi-objective optimization matching of the system. Compared with the existing methods in the literature, the main research contents and innovations of this paper are as follows:

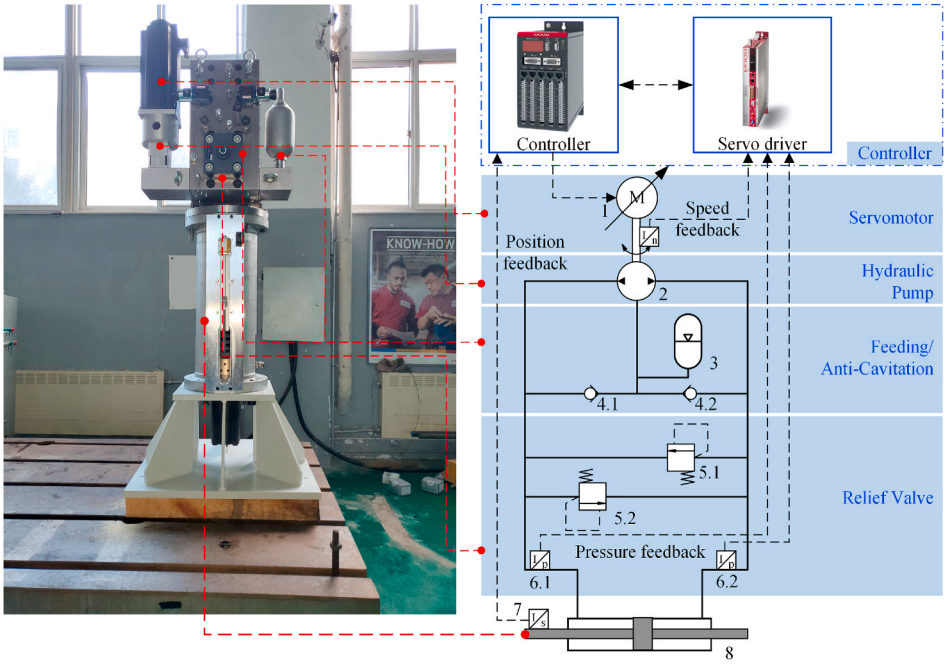

1-Servo motor, 2-Fixed displacement pump, 3-Accumulator, 4.1-One-way valve of oil cavity A, 4.2-One-way valve of oil cavity B, 5.1-Relief valve of oil cavity A, 5.2-Relief valve of oil cavity B, 6.1-Pressure transducer of oil cavity A, 6.2-Pressure transducer of oil cavity A, 7-Displacement transducer, 8-Hydraulic cylinder

Fig. 1. Working principle of the EHSPCS.

1) Aiming at the dynamic and efficient energy-saving characteristics of the EHSPCS, an evaluation model for the dynamic and thermal power characteristics of key components of the system is established. The optimized quantitative indicators are refined to lay the foundation for multi-objective optimization of the EHSPCS.
2) Taking the dynamic cycle of the hydraulic cylinder and the thermal power loss of the servo motor as the objective function, the parameters such as the electromagnetic torque of the servo motor, the displacement of the hydraulic pump, and the working area of the hydraulic cylinder are intelligent optimized by using the non-dominated sorting genetic algorithm with elitist strategy (NSGA-II). The Pareto frontier of multi-objective optimization and the corresponding Pareto solution set are obtained, and realize the optimal matching of dynamic and efficient energy-saving characteristics.
3) The relevant theory of multi-objective optimization algorithm is formed into the key technology, applied to the optimization of the performance parameters of the hydraulic servo motor. The engineering test of the prototype is carried out to provide a theoretical basis and guidance for the design and optimization of the EHSPCS.

2. Working principle of the EHSPCS

The EHSPCS adopts a servo motor-fixed displacement pump-hydraulic cylinder volume control scheme. The servo motor coaxially drives the fixed-displacement pump, and the suction and discharge ports of the pump are directly connected to the two load ports of the hydraulic cylinder. The accumulator cooperates with one-way valves to realize the oil-filling function of the system. The relief valves realize overload protection of the system pressure. The displacement and pressure signals from the hydraulic cylinder are collected and compared with the input signals by the controller, and speed and torque instructions are outputted to the servo motor. Thus the high-precision control of the displacement and force is realized. The composition and working principles of the EHSPCS are shown in Fig. 1.

3. Analysis of high efficiency and high dynamic characteristics of the EHSPCS

The dynamic period and thermal power loss of the system are analyzed according to the dynamic and efficient energy-saving characteristics of the EHSPCS. Then, the optimized quantitative indices are extracted, which lays the foundation for multi-objective optimization and coordinated matching of the system.

3.1. Analysis of dynamic characteristics

In the working process of the EHSPCS, it is assumed that the hydraulic cylinder and the load work in the high-frequency dynamic running state to study its dynamic characteristics. The sinusoidal tracking performance is selected to analyze the dynamic characteristics of the system. The displacement curve of the hydraulic cylinder is expressed as Eq. (1):

$$x_p = b\sin(2\pi ft) \tag{1}$$

where b is the sinusoidal signal amplitude, f is the sinusoidal signal operating frequency, and t is the movement time of the hydraulic cylinder.

Further, the running speed of the hydraulic cylinder can be represented as Eq. (2):

$$v_p = \frac{dx_p}{dt} = 2\pi fb\gamma\cos(2\pi ft) \tag{2}$$

where γ is the attenuation ratio of the amplitude value of the hydraulic cylinder.

The load characteristics of the EHSPCS vary in real time. If the actual load is equivalent to the combination of the inertial, viscous damping load, and elastic loads, the actual workload can be shown as Eq. (3):

$$\begin{aligned} F_q &= m\ddot{x}_p + B_p\dot{x}_p + Kx_p \\ &= \left(K - m\omega^2\right)b\sin\omega t + B_p\omega b\gamma\cos\omega t \end{aligned} \tag{3}$$

where m denotes the load quality, K denotes the stiffness of the load spring, B_p denotes the viscous damping coefficient, and ω denotes the angular velocity of the sine signal.

The system workload is converted to servomotor torque, and the equivalent load torque is expressed as Eq. (4):

$$T_L = \frac{D_p F_q}{A_p} \tag{4}$$

where D_p is the hydraulic pump displacement and A_p is the working area of the hydraulic cylinder.

Because the viscous damping coefficient is small and negligible, the equivalent load torque can be presented as Eq. (5):

$$T_L = \frac{D_p}{A_p}\left(K - m\omega^2\right)b\sin\omega t \tag{5}$$

In this motion mode, the liquid flow required for the movement of the hydraulic cylinder is shown in Eq. (6):

$$Q_L = v_p A_p = 2\pi f b A_p \gamma \cos(2\pi f t) \tag{6}$$

Ignoring the influence of system leakage and oil compression characteristics, the angular and rotational speeds of the corresponding servo motor can be expressed as Eq. (7):

$$\begin{cases} \omega_m = \dfrac{Q_1}{D_p} = \dfrac{2\pi f b A_p \gamma}{D_p} \cos(2\pi f t) \\ n_m = \dfrac{60\omega_m}{2\pi} = \dfrac{60 f b A_p \gamma}{D_p} \cos(2\pi f t) \end{cases} \tag{7}$$

Furthermore, the corresponding angular acceleration and acceleration torque of the servo motor are presented as Eq. (8):

$$\begin{cases} \alpha_m = \dfrac{d\omega_m}{dt} = \dfrac{(2\pi f)^2 b A_p \gamma}{D_p} \sin(2\pi f t) \\ T_m = J_{mp}\alpha_m = \dfrac{J_{mp}(2\pi f)^2 b A_p \gamma}{D_p} \sin(2\pi f t) \end{cases} \tag{8}$$

where J_{mp} is the rotor inertia of motor pump group.

From Eqs. (5) and (8), it is known that the working torque of the servo motor is represented as Eq. (9):

$$T_e = T_L + T_m = \left[\frac{D_p}{A_p}\left(K - m\omega^2\right)b + \frac{J_{mp}\omega^2 b A_p \gamma}{D_p}\right] \sin \omega t \tag{9}$$

Set the hydraulic speed ratio as Eq. (10):

$$\lambda = \frac{D_p}{A_p} \tag{10}$$

Then Eq. (10) can be written as Eq. (11):

$$T_e = \lambda b\left(K - m\omega^2\right) \sin \omega t - \frac{J_{mp}\omega^2 b\gamma}{\lambda} \sin \omega t = \left[\lambda b\left(K - m\omega^2\right) - \frac{J_{mp}\omega^2 b\gamma}{\lambda}\right] \sin \omega t \tag{11}$$

The load curve of the servo motor is shown in Eq. (12):

$$\left(\frac{T_e}{\lambda b\left[K - m(2\pi f)^2\right] - \frac{J_{mp}(2\pi f)^2 b\gamma}{\lambda}}\right)^2 + \left(\frac{n_m D_p}{60 f b A_p \gamma}\right)^2 = 1 \tag{12}$$

From Eq. (12), the dynamic frequency expression of the system can be obtained as Eq. (13):

$$f = \frac{1}{2\pi}\sqrt{\frac{T_e - \lambda b K}{\frac{J_{mp} b\gamma}{\lambda} + \lambda b m}} \tag{13}$$

Then the dynamic periodic expression of the system is expressed as Eq. (14):

$$T = \frac{1}{f} = 2\pi\sqrt{\frac{\frac{J_{mp} b\gamma}{\lambda} + \lambda b m}{T_e - \lambda b K}} \tag{14}$$

The dynamic period of the system is selected as its dynamic performance index, as shown in Eq. (14). The factors that affect the dynamic characteristics of the system include the electromagnetic torque of the servo motor, hydraulic speed ratio (hydraulic pump displacement, hydraulic cylinder area), rotor inertia of the motor pump group, load spring stiffness, and load mass. The specific relationships are as follows.

1) The electromagnetic torque of the servo motor is positively correlated with the dynamic characteristics of the system;
2) The rotor inertia, load spring stiffness and load mass of the motor pump group are negatively correlated with the dynamic characteristics of the system;
3) The hydraulic speed ratio (hydraulic pump displacement, hydraulic cylinder area) has a complex nonlinear relationship with dynamic characteristics.

3.2. Analysis of efficient energy-saving characteristics

The core of efficient energy-saving of the EHSPCS is reducing the energy loss and improving the working efficiency. The servo motor is key to the power loss of the system. During the working process, the power loss of the servo motor is dissipated in the form of thermal energy, which not only causes a large amount of energy loss but also reduces the service life of the motor and affects its

dynamic output capacity.

The thermal power loss of the servo motor is selected as the index of efficient energy-saving characteristics, which reflects the overall energy loss of the system through the thermal power loss of the servo motor and then indirectly reflects the efficient energy-saving characteristics of the system.

The thermal power loss of servo motor can be expressed as Eq. (15):

$$P_{\text{loss}} = mI^2R + k_{\text{r}}C_{\text{m}}\rho\omega^3 r^4 l + \left(k_{\text{c}}f^2B_{\text{m}}^2 + k_{\text{h}}fB_{\text{m}}^{\beta} + k_{\text{e}}f^{1.5}B_{\text{m}}^{1.5}\right) \tag{15}$$

To facilitate the analysis of the thermal power loss, Eq. (15) is transformed into Eq. (16):

$$P_{\text{loss}} = k_1 I^2 + k_2\omega_{\text{m}} + k_3\omega_{\text{m}}^2 + k_4\omega_{\text{m}}^3 \tag{16}$$

As can be seen from Eq. (16), starting from the working physical parameters of the servo motor, the thermal power loss of the servo motor mainly depends on the working current and motor speed. The working current and motor speed are associated with the system working parameters in section 3.1, which can be shown in Eq. (17):

$$\begin{cases} I = \dfrac{T_e}{K\text{t}} \\ \omega_{\text{m}} = \dfrac{2\pi fb\gamma}{\lambda}\cos(2\pi ft) \end{cases} \tag{17}$$

where K_{t} is the conversion coefficient of phase current and electromagnetic torque.

From Eqs. (16) and (17), it can be seen that the factors of efficient energy-saving characteristics include servo motor electromagnetic torque, hydraulic speed ratio (hydraulic pump displacement, hydraulic cylinder area), system working frequency and so on. The electromagnetic torque of the servo motor and the working frequency are positively correlated with the power loss, which weakens the efficient and energy-saving characteristics; the hydraulic speed ratio is negatively correlated with the power loss, which improves the efficiency energy-saving characteristics.

According to the analysis of the system dynamic and efficient energy-saving characteristics in sections 3.1 and 3.2, the constraints of electromagnetic torque of the servo motor, hydraulic speed ratio (hydraulic pump displacement, hydraulic cylinder area) and other components are often contradictory. Good dynamic characteristics require a higher electromagnetic torque of the servo motor to improve the dynamic output capacity. However, a higher electromagnetic torque increases the working current and aggravates the thermal power loss of the servo motor, thus affecting the efficient energy-saving characteristics. Therefore, the component parameters are difficult to meet the requirements of dynamic characteristics and efficiency energy-saving characteristics at the same time, so it is necessary to carry out multi-objective optimization and coordinated matching between them.

4. Multi-objective optimization mathematical model of EHSPCS

The flowchart of the multi-objective optimization method for the EHSPCS is shown in Fig. 2. The optimization process can be divided into three phases: modeling, multi-objective optimization, and experimental verification.

Multi-objective optimization of the performance indices is carried out by MATLAB. Firstly, the physical model of the design

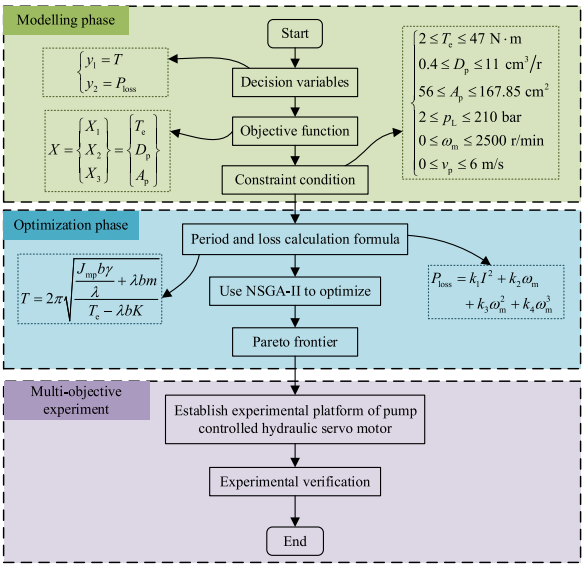

Fig. 2. The flow chart of the multi-objective optimization design of EHSPCS.

problem can be transformed into a mathematical model, which includes three aspects: the objective function, decision variables, and constraints. The decision variable is the independent variable and the objective function is the dependent variable. Simultaneously, the objective function expresses the relationship between the optimal index and decision variable, and the constraint condition expresses the range of the decision variable and objective function. The following mathematical expression is used to describe multi-objective optimization.

Decision variables can be expressed as Eq. (18):

$$x = (x_1 + x_2 + ... + x_n)^T \tag{18}$$

Objective function is shown in Eq. (19):

$$\min y(x) \quad x \in R^n \tag{19}$$

Constraint condition is presented as Eq. (20):

$$\begin{cases} p_i(x) \geq 0 \quad i = 1, 2, 3, ..., m \\ q_i(x) = 0 \quad i = 1, 2, 3, ..., k \end{cases} \tag{20}$$

4.1. Objective function

The objective of multi-objective optimization design is to determine the optimal solution from the feasible region. Combined with the efficient energy-saving and dynamic characteristics of the EHSPCS, and the principle of selecting the smaller the better in the multi-objective optimization, the dynamic period of the hydraulic cylinder and the thermal power loss of the servo motor are selected as the objective functions. Then, the goal of the minimum period and minimum loss is achieved as Eq. (21):

$$\begin{cases} y_1 = T \\ y_2 = P_{loss} \end{cases} \tag{21}$$

4.2. Decision variables

From the above analysis, it can be seen that the dynamic and efficient energy-saving characteristics of the system are closely related to the electromagnetic torque of the servo motor, displacement of the hydraulic pump, and working area of the hydraulic cylinder. To achieve the best match between these two characteristics, the working torque of the servo motor, displacement of the hydraulic pump, and working area of the hydraulic cylinder are selected as decision variables. The rotor inertia of the motor pump group, load spring stiffness, load quality and amplitude of the sinusoidal signal of the hydraulic cylinder are selected as the basic constants.

Based on the physical parameters of the hydraulic servo motor, and considering the correlation and constraints among them, the values (range) of the decision variables and basic constants are listed in Table 1.

4.3. Constraint condition

In order to ensure the feasibility of the optimization results, when optimizing the performance of the system, it is necessary to limit the basic physical parameters of the system according to the actual working conditions and set constraints.

Considering the pressure strength design of hydraulic components, the load pressure p_L of the system is between 2–210 bar. According to the rated speed range of servo motor, the working speed ω_m of servo motor is between 0–2500 r/min. Considering the maximum linear speed limit of cylinder seal, the running speed v_p of hydraulic cylinder is between 0 and 6 m/s.

4.4. Optimal matching mathematical model

Considering the characteristics of dynamic and efficient energy-saving, the multi-objective optimization matching mathematical model of the system is described as Eq. (22):

Table 1
Value table of decision variables and basic constants.

Physical quantity		Symbol	Value (range)
Decision variable	Electromagnetic torque of servo motor (N·m)	T_e	[2,47]
	Hydraulic pump displacement (mL/r)	D_p	[0.4,11]
	Working area of hydraulic cylinder (cm^2)	A_p	[56,167.85]
Basic constant	Rotor inertia of motor pump group (kg·cm^2)	J_{mp}	20
	Load spring Stiffness (N/m)	K	5×10^4
	Load quality (kg)	m	50
	Amplitude of sine signal of hydraulic cylinder (m)	b	0.01

$$
\begin{aligned}
&find\ x = \left[T_e, D_p, A_p\right]^T \\
&\begin{cases}
\min\left\{T\left(T_e, D_p, A_p\right), P_{loss}\left(T_e, D_p, A_p\right)\right\} \\
s.t. \quad 2 \le T_e \le 47 \\
\quad 0.4 \le D_p \le 11 \\
\quad 56 \le A_p \le 167.85 \\
\quad 2 \le p_L \le 210 \\
\quad 0 \le \omega_m \le 2500 \\
\quad 0 \le v_p \le 6
\end{cases}
\end{aligned} \tag{22}
$$

5. Non-dominated sorting genetic algorithm based on the elite strategy

In this paper, the dynamic period T of the hydraulic cylinder and the total loss of thermal power P_{loss} are selected as the objective functions. The objective functions are mutually restricted by decision variables. The optimization of one objective must be at the cost of reducing the characteristics of another objective, which belongs to the multi-objective optimization problem. The solution to a multi-objective optimization problem is not a single solution, but an optimal set called the Pareto solution set. The optimization problem in this paper is designed for EHSPCS, which is a continuous problem. The non-dominated sorting genetic algorithm based on elitist strategy (NSGA-II) is suitable for the optimization of continuous problems, and has the advantages of fast running speed and good convergence. Based on the selection of the optimization variables, the non-dominant sorting genetic algorithm based on the elite strategy (NSGA-II) introduces fast non-dominant sorting, elite retention, and congestion comparison methods. It significantly improves the convergence speed of the iteration, reduces the computational complexity, and ensures the diversity of the population [25,26]. The principle of the NSGA-II genetic algorithm is shown in Fig. 3, and its basic steps are as follows.

Step 1: According to the different values of the optimization variables, the initial sample population P_t (t = 0) with size N is randomly generated. The fitness value of each individual (the indices of dynamic and efficient energy-saving characteristics) is calculated.
Step 2: Fast non-dominant ranking of the sample population is performed. The non-dominant solution set is selected from the sample population, and Level 1 is assigned; subsequently, these individuals are removed from the population. A new non-dominant solution set is selected from the remaining individuals and assigned to Level 2. All the individuals in the population are ranked in the same manner. The crowding distance of individuals at the same level is calculated. The crowding distance definition of individual i is shown in Fig. 4, and the calculation method is expressed as Eq. (23) [27]:

$$
d_i = \sum_{j=1}^{k} \left| \frac{f_j^{i+1} - f_j^{i-1}}{f_j^{\max} - f_j^{\min}} \right| \tag{23}
$$

where d_i is the crowding distance of the individual, k is the number of objective functions, f_j^{i+1} is the value of the j objective function of individual $i+1$, f_j^{i-1} is the value of the j objective function of individual i-1, $f_j^{\max}$ is the maximum value of objective function j, and $f_j^{\min}$ is the minimum value of objective function j.

Step 3: Through binary tournament selection, crossover, and mutation operations on the sample population, the subsample population Q_t ($t = 0$) is obtained.
Step 4: By combining the sample population P_t and Q_t, the sample population R_t with size 2 N is obtained, the sample population R_t is ranked, and the non-dominant solution set (F1, F2, F3, …) is obtained. The crowding distance for every individual is calculated.

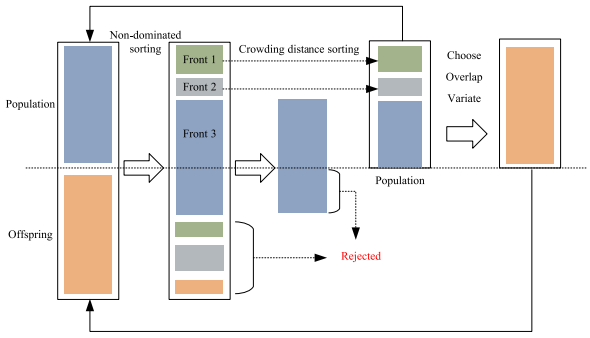

Fig. 3. Schematic diagram of NSGA-II algorithm.

Step 5: According to the hierarchy and crowding distance, the optimal N individuals are selected to form a new sample population P_t+1. When selecting, priority is given to individuals at lower levels, and individuals with large crowding distance are selected for individuals at the same level.

Step 6: The selection, crossover and mutation operations are performed on the sample population P_t+1 to produce a new subsample population Q_t+1 of size N.

Step 7: If the termination criteria are met, the iteration ends; otherwise, go to Step 4 to continue the execution.

6. Optimization result and analysis

Based on the high-efficiency and high-dynamic evaluation model of the EHSPCS, the objective function and decision variables of NSGA-II algorithm are compiled by MATLAB. The number of populations is set to 100, and the number of iterations is 10,000. After the optimization and iterative calculation, the Pareto front of the multi-objective optimal matching of the pump control system is obtained, as shown in Fig. 5a. The multi-objective particle swarm algorithm (MPSO) has a good global search capability and is widely used in the optimization of engineering machinery. The Pareto front are obtained after 10,000 iterations of optimization using NSGA-II and MPSO, which is shown in Fig. 5b. From Fig. 5b, it can be found that the optimization effect of NSGA-II is better than MPSO overall in this case. The design solution will be selected from the Pareto front obtained by NSGA-II.

From the Pareto front of the multi-objective optimization of the system, it can be found that the range of the dynamic period (s) of the hydraulic cylinder is [0.314, 0.748], and the range of power loss (W) of the servo motor is [21.6, 665.0]. The values of these two objective functions cannot be optimized simultaneously, one objective function is optimized at the expense of the other. Therefore, the required 'optimal solution' can be determined according to the optimization preference of the actual working conditions of the system. For example, in engineering, we usually prioritized to put forward the dynamic characteristic requirements of the system from the perspective of high-performance control and then determine the dynamic cycle index. Finally, we obtain the corresponding optimal solution in the Pareto front. The distribution of each decision variable in the multi-objective optimization Pareto solution set is shown in Fig. 6.

Fig. 6 shows the distribution of decision variables corresponding to the Pareto frontier. As shown in Fig. 6a, the range of electromagnetic torque (N·m) in the Pareto solution set is [7.5, 47.5], in which there are more particles in the interval [7.5, 12.5], and the number of particles decreases with the increase in torque. As shown in Fig. 6b, the displacement (mL/r) of the hydraulic pump is mainly concentrated between [6.25, 6.5]. As shown in Fig. 6c, the value of the working area (cm^2) of the hydraulic cylinder is mainly distributed between [55, 60].

The hypervolume index (HV) is selected to evaluate the multi-objective optimization results of the system. HV characterizes the hypervolume surrounded by the points in population P_t and reference point set R_t. The higher the HV value, the better the convergence and distribution of the algorithm and the higher the comprehensive performance. The corresponding HV values obtained in this study are shown in Fig. 7.

As shown in Fig. 7, after 4000 iterations, the HV index reaches 95%, indicating that the NSGA-II optimization algorithm proposed in this study has good comprehensive performance in the process of optimizing the system dynamic and efficient energy-saving characteristics.

7. Application and experimental verification of multi-objective optimization result

The related theory of multi-objective optimal matching of the EHSPCS is developed and applied to the optimal matching of dynamic and efficient energy-saving characteristics of hydraulic servo motors. A test platform of the hydraulic servo motor is built, and the prototype is tested in engineering to verify the feasibility and effectiveness of the proposed theory.

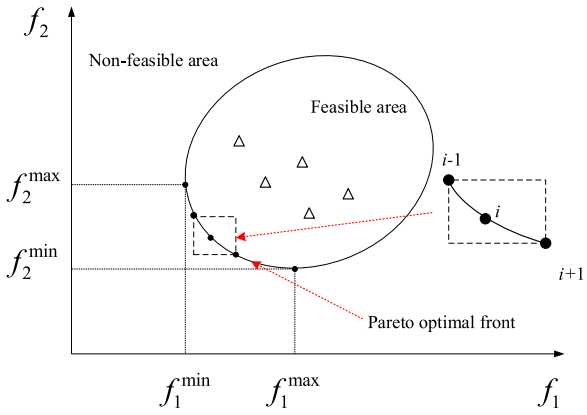

Fig. 4. Method of crowding distance determination.

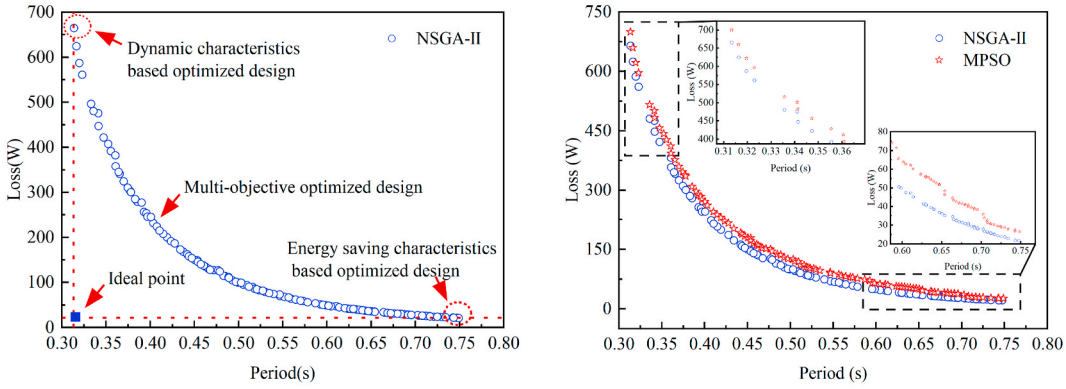

(a) NSGA-II (b) NSGA-II vs MPSO

Fig. 5. Pareto front of multi-objective optimization.

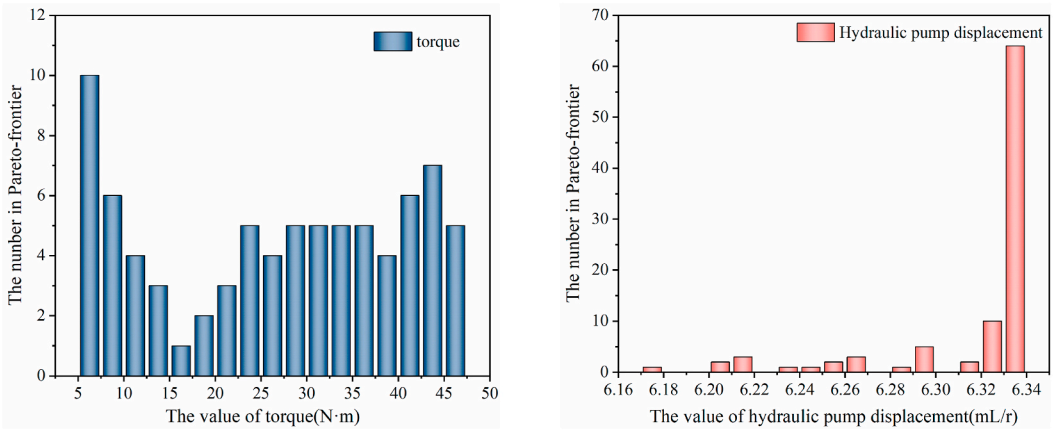

(a) Distribution of torque in the Pareto frontier

(b) Distribution of hydraulic pump displacement in the Pareto frontier

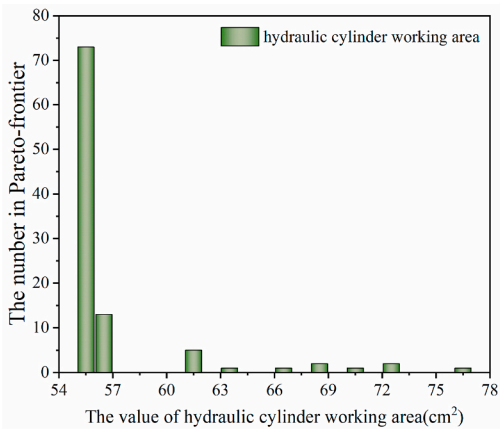

(c) Distribution of hydraulic cylinder working area in the Pareto frontier

Fig. 6. Pareto front of optimization results of EHSPCS.

7.1. Overview of the hydraulic servo motor

The hydraulic servo motor is a hydraulic actuator formed by an EHSPCS. As an important component of the steam turbine unit, it changes the air intake of high-pressure steam by adjusting the steam intake valve and then regulates the power of the unit. It plays a

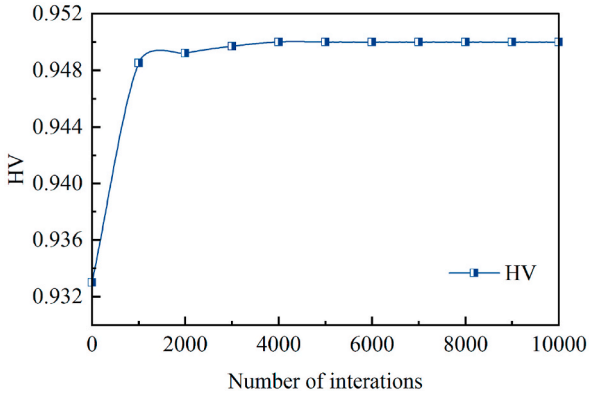

Fig. 7. HV evaluation index of multi-objective optimization.

vital role in improving the working performance of the unit. In this study, a hydraulic servo motor is used as an experimental platform to verify the proposed theory.

7.2. Multi-objective optimization of performance parameters of the hydraulic servo motor

It is known that the initial values of the structural parameters of the hydraulic servo motor are $T_e = 25$ N m, $D_p = 10$ mL/r and $A_p = 105$ cm^2, substituting Eqs. (14) and (16), the calculated result in the Pareto front is shown in Fig. 8. It is obvious that the point is not on the Pareto front, the initial value does not belong to the optimal solution. The dynamic and efficient energy-saving characteristics need to be further optimized.

By optimizing the relevant parameters of the electromagnetic torque T_e, hydraulic pump displacement D_p, and hydraulic cylinder working area A_p, the working point of the system is within the optimal solution range of the Pareto front. According to the requirements of the hydraulic servo motor control process, priority should be given to the dynamic characteristic requirements of the system (considered as 2 Hz) to ensure the dynamic response ability. Select (0.48, 148) in the Pareto frontier as the optimal design scheme for the hydraulic servo motor. Further considering the existing product specifications such as servo motors and quantitative pumps, the parameters of the corresponding optimized hydraulic servo motor are shown in Table 2.

Based on the above solution set, the technical requirements of the hydraulic servo motor in Table 3 are checked. The output of the hydraulic cylinder and motor drive meet the technical requirements, and the optimized solution meets the process requirements.

7.3. Build the test platform of hydraulic servo motor

A hydraulic servo motor test platform is set up. A typical sinusoidal signal is selected as the speed instruction of the servo motor so that the hydraulic cylinder and load are dynamically output. The measured values are compared with the theoretical values of multi-objective optimization to verify the effectiveness and feasibility of the proposed multi-objective method. The overall test platform is illustrated in Fig. 9. The servo motor, fixed-displacement pump, hydraulic valves, and sensors are integrated into the hydraulic cylinder through a functional valve block. The hydraulic cylinder is connected to a mechanical spring through the control seat. The

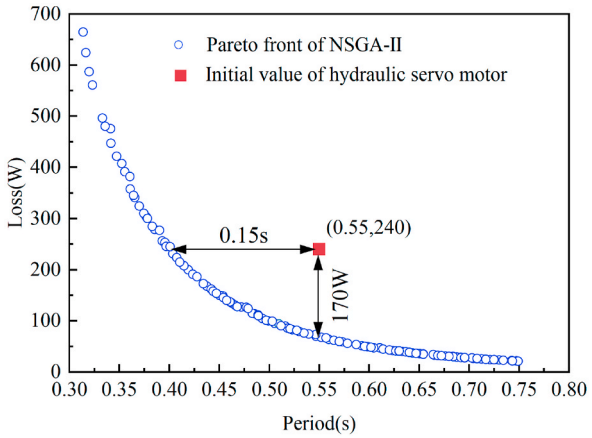

Fig. 8. Initial value of hydraulic servo motor.

Table 2
Optimal design decision variables and objective function of hydraulic servo motor.

Objective function		Decision variable		
P_{loss} (W)	T (s)	T_e (N·m)	D_p (mL/r)	A_p (cm^2)
148	0.48	23.5	6.3	72

Table 3
Technical index requirements of hydraulic servo motor.

Serial number	Name	Parameters	Unit
1	Rated working pressure	14	MPa
2	Cylinder output	150	kN
3	Work schedule	65	mm
4	Pre-loading	49.4	kN
5	Rated load	75	kN
6	Position control accuracy	±0.05	mm
7	Working medium	Phosphate ester fire resistant oil	/

electric control cabinet integrates important electrical components such as the shaft controller, servo driver, and isolation module. The technical specifications of the hydraulic servo motor are shown in Table 4.

The sine signal instruction is given to the servo motor, the experimental curves of dynamic characteristics and efficient energy-saving characteristics of the hydraulic servo motor are shown in Fig. 10. During the dynamic output process of the system, the hydraulic cylinder is dynamically adjusted with the servo motor speed instruction. The dynamic cycle of the hydraulic cylinder is 0.56s and the average thermal power loss of servo motor is about 245.6 W, which is basically consistent with the theoretical calculation value. After using the multi-objective optimization matching method, the dynamic cycle of the hydraulic cylinder can reach 0.5s and the optimization ratio can reach 10.7%, the average thermal power loss of the servo motor is about 150.4 W and the optimization ratio can reach 38.8%. It is consistent with the simulation value (the dynamic cycle of the hydraulic cylinder is 0.48s and the thermal power loss of the servo motor is 148 W). The feasibility and effectiveness of the optimization matching theory of dynamic characteristics and efficient energy-saving characteristics are further verified.

8. Conclusion

The multi-objective optimal matching of the EHSPCS dynamic and efficient energy-saving characteristics is investigated in this study. The important performance parameters of the EHSPCS are analyzed. The electromagnetic torque of the servo motor, displacement of the hydraulic pump, and working area of the hydraulic cylinder are selected as the decision variables. The dynamic period of the hydraulic cylinder and total loss of the servo motor are selected as the objective functions. A multi-objective optimization strategy based on the NSGA-II genetic algorithm is proposed, the multi-objective optimization Pareto front and Pareto solution set are obtained. The optimal design scheme of the EHSPCS is gained. Optimal matching of the system dynamic and efficient energy-saving characteristics is received. The multi-objective optimization results are also applied successfully to the coordinated matching of the hydraulic servo motor performance parameters. Theoretical analysis and experimental tests show that the dynamic period after optimization is increased by 10.7%, and the thermal power loss is reduced by 38.8%. This study provides a theoretical and technical foundation for the performance optimization of the EHSPCS.

Author contribution statement

Guishan Yan: Conceived and designed the experiments; Contributed reagents, materials, analysis tools or data.
Mingkun Yang: Conceived and designed the experiments; Performed the experiments; Wrote the paper.
Yuhang Zhang: Conceived and designed the experiments; Wrote the paper.
Tiangui Zhang: Performed the experiments.
Chao Ai: Analyzed and interpreted the data.

Funding statement

This work was supported by National Natural Science Foundation of China [No. 52275066], Key R&D projects of Hebei Province (20314402D).

This work was supported by the Key R&D projects of Hebei Province [No. 20314402D].

Data availability statement

Data will be made available on request.

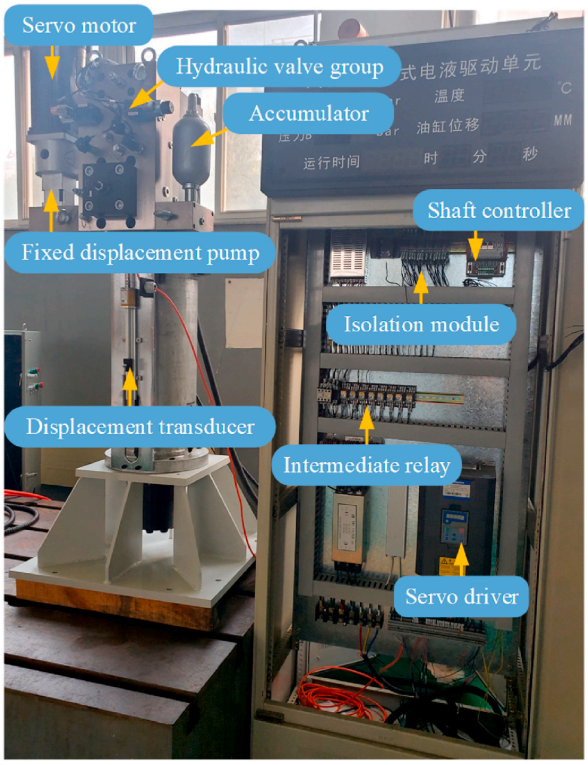

Fig. 9. The test platform of hydraulic servo motor.

Table 4
Technical specifications and parameters of hydraulic servo motor.

Serial number	Element	Name	Parameter
1	Servo Motor	Model	HP11321-G202A
		Rated torque	23.5 N·m
		Rated speed	3000r/min
2	Hydraulic pump	Model	TFH-630-U-PCV-F
		Displacement	6.3mL/r
		Rated working pressure	210 bar
3	Hydraulic cylinder	Model	Φ125/Φ80mm
		Stroke	70 mm
		Working area	72 cm^2

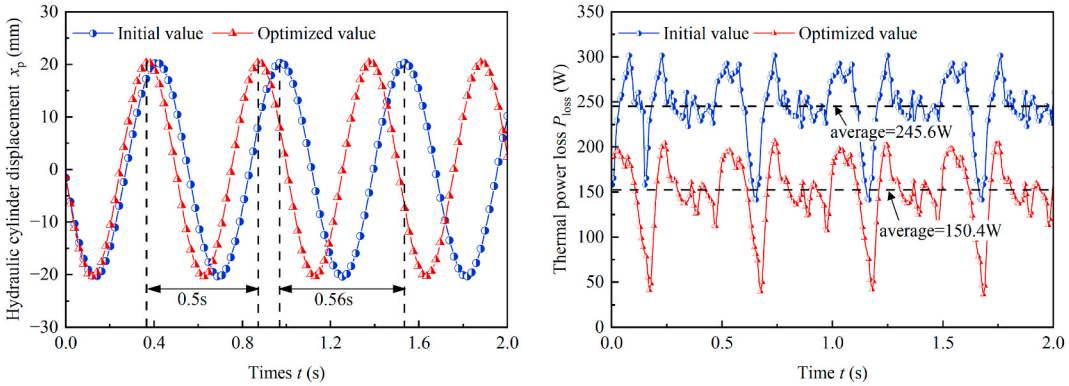

a) Hydraulic cylinder displacement b) Thermal power loss of servo motor

Fig. 10. Experimental comparison curve of the hydraulic servo motor.

Declaration of interest's statement

The authors declare no conflict of interest.

References

[1] I. Chakraborty, D.N. Mavris, M. Emeneth, A. Schneegans, A methodology for vehicle and mission level comparison of more electric aircraft subsystem solutions: application to the flight control actuation system, Proc. IME G J. Aero. Eng. 229 (6) (2015) 1088–1102, https://doi.org/10.1177/0954410014544303.

[2] C. Shi, X. Wang, S. Wang, J. Wang, M.M. Tomovic, Adaptive decoupling synchronous control of dissimilar redundant actuation system for large civil aircraft, Aero. Sci. Technol. 47 (2015) 114–124, https://doi.org/10.1016/j.ast.2015.09.012.

[3] B. Yu, S. Wu, Z. Jiao, Y. Shang, Multi-objective optimization design of an electrohydrostatic actuator based on a particle swarm optimization algorithm and an analytic hierarchy process, Energies 11 (9) (2018) 2426–2440, https://doi.org/10.3390/en11092426.

[4] L. Ge, L. Quan, Y. Li, X. Zhang, J. Yang, A novel hydraulic excavator boom driving system with high efficiency and potential energy regeneration capability, Energy Convers. Manag. 166 (2018) 308–317, https://doi.org/10.1016/j.enconman.2018.04.046.

[5] X. Yin, W. Zhang, Z. Jiang, L. Pan, Adaptive robust integral sliding mode pitch angle control of an electro-hydraulic servo pitch system for wind turbine, Mech. Syst. Signal Process. 133 (2019) 105704–105718, https://doi.org/10.1016/j.ymssp.2018.09.026.

[6] Z. Li, Y. Shang, Z. Jiao, Y. Lin, S. Wu, X. Li, Analysis of the dynamic performance of an electro-hydrostatic actuator and improvement methods, Chin. J. Aeronaut. 31 (12) (2018) 2312–2320, https://doi.org/10.1016/j.cja.2018.03.014.

[7] S. Lee, Y. Hong, A dual eha system for the improvement of position control performance via active load compensation, Int. J. Precis. Eng. Manuf. 18 (7) (2017) 937–944, https://doi.org/10.1007/s12541-017-0111-7.

[8] J. Yao, P. Wang, Z. Dong, D. Jiang, T. Sha, A novel architecture of electro-hydrostatic actuator with digital distribution, Chin. J. Aeronaut. 34 (5) (2021) 224–238, https://doi.org/10.1016/j.cja.2020.08.012.

[9] W. Jiang, P. Jia, G. Yan, G. Chen, C. Ai, T. Zhang, K. Liu, C. Jia, W. Shen, Dynamic response analysis of control loops in an electro-hydraulic servo pump control system, Processes 10 (8) (2022) 1647–1666, https://doi.org/10.3390/pr10081647.

[10] L. Huang, T. Yu, Z. Jiao, Y. Li, Research on power matching and energy optimal control of active load-sensitive electro-hydrostatic actuator, IEEE Access 9 (2021) 51121–51133, https://doi.org/10.1109/ACCESS.2020.3011629.

[11] O. Mesalhy, M.L. Elsayed, J.J. Corona Jr., A.A. Kwarteng, J.P. Kizito, Q.H. Leland, L.C. Chow, Study of a high-reliability dual-fan system for cooling aerospace electromechanical actuators, Therm. Sci. Eng. Prog. 18 (2020) 100540–100551, https://doi.org/10.1016/j.tsep.2020.100540.

[12] M. Yang, G. Chen, J. Lu, C. Yu, G. Yan, C. Ai, Y. Li, Research on energy transmission mechanism of the electro-hydraulic servo pump control system, Energies 14 (16) (2021) 4869–4885, https://doi.org/10.3390/en14164869.

[13] G.S. Yan, Z.L. Jin, M.K. Yang, B. Yao, The thermal balance temperature field of the electro-hydraulic servo pump control system, Energies 14 (5) (2021) 1364–1387, https://doi.org/10.3390/en14051364.

[14] S. Qu, D. Fassbender, A. Vacca, E. Busquets, A high-efficient solution for electro-hydraulic actuators with energy regeneration capability, Energy 216 (2021) 119291–119315, https://doi.org/10.1016/j.energy.2020.119291.

[15] K. Mccullough, Design and Characterization of a Dual Electro-Hydrostatic Actuator, McMaster University, Hamilton, 2011.

[16] J.F. Saldarriaga, Application of an artificial neural networks for predicting the heat transfer in conical spouted bed using the nusselt module, Heliyon 8 (11) (2022), https://doi.org/10.1016/j.heliyon.2022.e11611, 11611, 11615.

[17] L. Zhu, J. Qiu, M. Chen, M. Jia, Approach for the structural reliability analysis by the modified sensitivity model based on response surface function - kriging model, Heliyon 8 (8) (2022), https://doi.org/10.1016/j.heliyon.2022.e10046, 10046, 10058.

[18] L. Xue, S. Wu, Y. Xu, D. Ma, A simulation-based multi-objective optimization design method for pump-driven electro-hydrostatic actuators, Processes 7 (5) (2019) 274–287, https://doi.org/10.3390/pr7050274.

[19] L. Kong, X. Chen, J. Gong, D. Fan, B. Wang, S. Li, Optimization of the hybrid solar power plants comprising photovoltaic and concentrating solar power using the butterfly algorithm, Energy Convers. Manag. 257 (2022) 115310–115322, https://doi.org/10.1016/j.enconman.2022.115310.

[20] L. Hua, C. Zhang, T. Peng, C. Ji, M. Shahzad Nazir, Integrated framework of extreme learning machine (elm) based on improved atom search optimization for short-term wind speed prediction, Energy Convers. Manag. 252 (2022) 115102–115119, https://doi.org/10.1016/j.enconman.2021.115102.

[21] J. Zhang, Y. Shen, M. Gan, Q. Su, F. Lyu, B. Xu, Y. Chen, Multi-objective optimization of surface texture for the slipper/swash plate interface in eha pumps, Front. Mech. Eng. 17 (4) (2022) 48–51, https://doi.org/10.1007/s11465-022-0704-4.

[22] H.A. Suthar, J.J. Gadit, Multiobjective optimization of 2 dof controller using evolutionary and swarm intelligence enhanced with topsis, Heliyon 5 (4) (2019), https://doi.org/10.1016/j.heliyon.2019.e01410, 1410, 1437.

[23] H. Díaz, A.P. Teixeira, C. Guedes Soares, Application of Monte Carlo and fuzzy analytic hierarchy processes for ranking floating wind farm locations, Ocean Eng. 245 (2022) 110453–110462, https://doi.org/10.1016/j.oceaneng.2021.110453.

[24] C. Xu, Y. Ke, Y. Li, H. Chu, Y. Wu, Data-driven configuration optimization of an off-grid wind/pv/hydrogen system based on modified nsga-ii and critic-topsis, Energy Convers. Manag. 215 (2020) 112892–112909, https://doi.org/10.1016/j.enconman.2020.112892.

[25] K. Deb, M. Mohan, S. Mishra, Evaluating the ε-domination based multi-objective evolutionary algorithm for a quick computation of pareto-optimal solutions, Evol. Comput. 13 (4) (2005) 501–525, https://doi.org/10.1162/106365605774666895.

[26] Y. Tian, R. Cheng, X. Zhang, Y. Jin, Platemo: a matlab platform for evolutionary multi-objective optimization [educational forum], IEEE Comput. Intell. Mag. 12 (4) (2017) 73–87, https://doi.org/10.1109/MCI.2017.2742868.

[27] X. Yuan, M. Wang, J. Dong, Accelerated current-driven multi-objective topology optimization for compact ultrawide-band mimo antenna design, Heliyon 8 (11) (2022), https://doi.org/10.1016/j.heliyon.2022.e11548, 11548, 11553.